Stochastic Environmental Research and Risk Assessment
https://doi.org/10.1007/s00477-021-02110-0

ORIGINAL PAPER

A new methodology is outlined and demonstrated on the improvement of uncertainty and sensitivity analysis based on the random sampling method

Petr Pecha[1] · Miroslav Kárný[1]

Accepted: 1 October 2021

Abstract
In several hours of a calm meteorological situation, a relatively significant level of radioactivity may accumulate around the source. When the calm situation expires, a wind-induced convective movement of the air immediately begins. Random realisations of the input atmospheric dispersion model parameters for this CALM scenario are generated using Latin Hypercube Sampling scheme. The resultant complex random radiological trajectories, passing through both calm and convective stages of the release scenario, represent the necessary prerequisite for the prospective uncertainty analysis (UA) and the sensitivity analysis (SA). The novel approximation-based (*AB*) solution replaces the non-Gaussian sum of individual puffs at the end of the calm period with one Gaussian "super-puff" distribution. This substantially accelerates generation of a sufficiently large number of random realisations for the radiological trajectories, thus facilitating the subsequent UA and SA. Both of these procedures exploit a common mapping between the pairs of calculated output fields on the one hand and the realisation vectors of the associated random input parameters on the other hand. This paper presents the necessary technical background, as well as the idea of the *AB* solution and its use. Examples of 2-D random trajectories of deposited ^{137}Cs are presented in a graphical form. Global sensitivity analysis based on random sampling methods is outlined and improved feasibility o f the originally long-running computation is demonstrated.

Keywords Sensitivity study · Sampling-based methods · Random input parameters · Calm atmosphere · Radioactivity dissemination · Radioactive hot spots

1 Introduction

Discharges of chemical and radioactive substance harm human health and the environment. Industrial pollution takes on many faces. The activities causing pollution include burning coal, natural gas, untreated gas and liquid waste being released into the environment, improper disposal of chemical and radioactive wastes and many others. Chemical-plant failures or traffic accident during transport of chemicals are frequently described and documented. At the same time, a gradual accumulation of the industrial waste in the living environment leads to new demands on the risk analysis. An example of the necessity to re-evaluate the new harmful effect is the uranium food chain transport towards human body. The health effects of natural and depleted uranium are due to chemical effects and not due to the radiation. Kidney, bones and livers are the most vital target organs for uranium retention. Inhaled insoluble uranium compounds can also damage the respiratory tract. Contamination and risk assessment of heavy metals and uranium were widely studied from water and sediment samples. Uranium retention and respective irradiation doses from the ingestion pathway for a certain region in India are recently published by Bangotra et al. (2021).

This article deals with the accidents from the opposite side of the spectrum of the harmful release substances.

✉ Petr Pecha
pecha@utia.cas.cz

Miroslav Kárný
school@utia.cas.cz

[1] The Department of Adaptive Systems of the Institute of Information Theory and Automation, The Czech Academy of Sciences, v.v.i. Pod vodárenskou věží 4, 182 00 Prague 8, Czech Republic

Published online: 25 October 2021

Potentially dangerous process of radioactivity accumulation in the motionless (calm) atmosphere around the source of emission is examined. Ensuing transport into the surrounding environment caused by a sudden wind formation is modelled. This radioactivity release is called CALM scenario below. It consists of two temporal stages:

- *STAGE I* The gradual accumulation and dissipation of radioactive pollution that occurs locally around the point of release. It lasts several hours, T^{CALM}.
- *STAGE II* The instantaneous start of the wind that drifts and disperses the accumulated heap of radioactivity.

Meteorological conditions forecasted at the point of release affect the dispersion in both of these stages. Specifically, hourly data for nuclear power plant (NPP) localities provided by the Czech Hydro-Meteorological Service is used.

A deterministic analysis of such accidental release of radioactive substances into the motionless atmosphere followed by dissemination of the radioactivity by wind into the environment is presented in Pecha and Kárný (2021).

In STAGE I, the radioactive release is approximated by a long sequence of discrete discharges (instantaneous puffs) described with the aid of established 3-D formulae, e.g., Zannetti (1990); Pandey and Sharan (2019). The release proceeds under a zero horizontal wind speed. Each puff has a shape of an expanding discus with its centre at the pollution source. The 3-D Gaussian-puff distribution describes the radioactivity concentration in the air at the effective height. Time-dependent empirical relationships gained from field measurements under low wind speed serve for expressing its vertical and horizontal dispersion coefficients. The radioactivity depletion from the air—caused by physical mechanisms of radioactive decay, dry depletion and wet depletion—is implemented. At the end of the calm stage, the resulting distribution is the superposition of all puffs, each having its "age". This age is the travel time of the puff from its birth until the end of the calm period. The effect of low wind conditions and wind intervals on atmospheric dispersion factors are treated in Hyojoon et al. (2013).

In STAGE II, the convective transport induced by the wind immediately starts. Two alternative procedures for handling the convective transport are inspected:

Brute-force solution (BF) The movement of each individual Gaussian puff, labelled by $m \in \{1,..,M\}$, is modelled through the whole convective phase. The resulting radiological quantities are then given by the superposition for all M puffs within the entire calm interval. This procedure provides an exact physical picture. A heavy demand on computer resources is its drawback. It may make proper modelling of the calm stage impossible for large values of M.

Approximation based on Bayes' paradigm (AB) The demand on computer resources can be substantially decreased by projecting the non-Gaussian sum of all partial Gaussian puffs on a representative Gaussian "super-puff" distribution (cf. the details below). Unlike *BF*, it requires only one-shot run modelling of the convective transport. The benefit of the reduced computational load is evident, especially for a large number of puffs M and for applications of more powerful but laborious dispersion codes to the convective STAGE II. Such applications are envisaged as necessary. The reduction of the computational load is paid for by an approximation error. Sensitivity of the results to this error is to be checked. Detailed results of comparative analysis of the *AB* vs *BF* solutions are outlined in the Appendix. A good fit has been established for all tested variants.

The non-trivial basis of the *AB* method is based on a simple observation that the achieved quality of the gained projection depends on the proximity measure defining it. The example supporting this observation is the well-known fact that the Euclidean distance is not a good choice when planning the shortest path in a town with a net of perpendicular roads. In the *AB* case, a weighted sum of Gaussian probability density functions is to be approximated by a simpler probability density. Works by Bernardo (1979) and Kárný and Guy (2012) showed that (under different, but quite general, conditions) the specific-version of the asymmetric Kullback-Leibler divergence (Kullback and Leibler 1951) is the (only) adequate proximity measure.

The optimal approximant G^{opt} is searched for in the set $\boldsymbol{G}$ of candidates. This set G should consist of mixtures of Gaussian pdf having fewer than M terms but more than one, McLachlan and Peel (2000). This ideal case, however, makes the evaluation of the Kullback-Leibler divergence, and therefore its minimisation, quite demanding, Hershey and Olsen (2007). This has led us to the referred attempt to approximate the mixture by a single Gaussian probability density function. It can then simply be shown that the optimal approximating "super-puff" G^{opt} must preserve the first and second moments of the mixture to be approximated. The optimal projection thus becomes computationally inexpensive.

The convective transport in STAGE II, under low wind speed conditions with a wind speed < 1 [m.s-1], has suffered from a knowledge gap in its previous analysis. It was generally believed that the commonly used steady-state Gaussian dispersion models, such as AERMOD (EPA 2004) or ADMS, Carruthers et al. (2003), are not applicable to situations when the wind speed close to the ground

is comparable to the standard deviation of the horizontal velocity fluctuation. The performance of such Gaussian dispersion models was poor and the concentration values during low-wind speed episodes were highly over-estimated. An important new option exists that suppresses this drawback. This option increases the minimum horizontal turbulence and incorporates a modified meander component. It was compared with an application of the Lagrangian dispersion model, Rakesh et al. (2019) for the low wind speed conditions. The performance levels of the Gaussian model with improved dispersion parameters and a specific Lagrangian dispersion model are in good mutual agreement. A profound overview of the significant references and methodology improvements are in Pandey and Sharan (2019).

Concerning the codes suitable to STAGE II, a wide range of various dispersion codes can be applied provided that the necessary input data is available and the computation load is bearable. The classical Gaussian approach, e.g., Adriaensen (2002), is still alive and successfully applied in many branches. More computationally demanding but more accurate Lagrangian dispersion models are naturally suitable for such problems. The Lagrangian particle dispersion model tracks each "point-like" particle of the pollution on its path through atmosphere. The particles drift with the mean wind velocity. They additionally undergo a random turbulence. Eulerian dispersion models solve the pollutant problem described by the diffusion equation on a fixed 3-D Cartesian equidistant computation grid. The Eulerian approach is computationally expensive and requires complex input data.

The practical choice of the dispersion code constitutes a compromise between the modelling objective and the achievable accuracy. The main objective is a design of computer code that would be as fast as possible and accurate enough for multi-fold repetitive sequential Monte Carlo calculations. They run for many-thousand realisations of random model parameters. These runs are necessary prerequisites for the uncertainty and sensitivity analysis, probabilistic assessment of potential radiological consequences and application of advanced statistical assimilation techniques of Bayesian filtering, e.g., Pecha and Hofman (2007). From this point of view, a fast generation of random radiological trajectories of the calm scenario consisting of STAGE I and STAGE II plays a decisive role. The advantage of *AB* approximation against *BF* solution is then vital.

This paper demonstrates the discussed aspect on a simple scenario for the real calm situation when radioactive pollution is discharged into motionless surroundings. The commonly used algorithms for a Gaussian puff model with the puff segmented modification suits the demonstration purposes. Drifting of the hourly pollution segments is driven by hourly meteorological forecasts. A detailed description is given in *(HARP,* 2010-*2021),* Section *Applications of the HARP system in radiation and chemical protection*.

2 Probabilistic approach of the CALM scenario

Our investigation, oriented on the probabilistic analysis of the CALM scenario, relies on the existing deterministic processing. The high-performance tool for uncertainty and sensitivity studies is obtained thanks to the novel "super-puff" concept of *AB*. These studies can be performed with the aid of the sampling-based Monte Carlo procedures requiring a very high number of random samples.

First, we recall the difference between variability and uncertainty of a quantity. Variability reflects its changes over time, over space or across individuals in a population. Variability represents diversity or heterogeneity in a well-characterised population. The term "uncertainty" covers stochastic or structural uncertainties representing partial ignorance or incomplete knowledge associated with the lack of perfect information about poorly-characterised phenomena or models. It applies also to model inputs and processing method.

For the selected dispersion model, many uncertainties related both to the conceptual model (parameterisation errors, uncertain sub-model parameters, stochastic nature of some measured input data, etc.) and the computational scheme (step of the computation net, the way the land-use characteristics are averaged, the averaging time for dispersion parameters, etc.) are involved. For a particular definition of the limited group of input random parameters and their ranking, we have accepted the former results used by the similar international environmental codes, e.g. UFOMOD, COSYMA, MARC-2A, OSCAAR, NPK-PUFF. The corresponding extensive literature review is given in Pecha and Pechova (2005). The used random characteristics should be regularly refreshed according to the recent recommendations provided by experts (this is a sensitive point of this study).

Formally, let $\mathbf{X} \equiv \{X_1, X_2, \ldots, X_N\}$ denote a vector of N random input model parameters X_i each having its distributions D_i, i = 1,…,N. Each input is characterised by its range, type of distribution, and potential mutual dependencies. The inputs are selected on the basis of commonly accepted agreement among experts (elicitation procedures). The output random fields from the CALM dispersion model can be schematically described as follows:

$$Y(A) = \Re^{CALM}(X_1, X_2, \ldots, X_N) \ldots \text{for dependent random variable Y at a single spatial point A (a scalar variable)} \quad (1a)$$

$$(\mathbf{Y}^k)_\Gamma = \Re^{CALM}(X_1, X_2, \ldots X_N) \ldots \text{for dependent random spatial field } Y^k \text{ (a vector of the output values of the field k determined on the polar calculation grid } \Gamma \quad (1b)$$

$$(Y^{k=1,\ldots K})_\Gamma = \Re^{CALM}(X_1, X_2, \ldots, X_N) \ldots \text{for dependent associated random spatial fields} \mathbf{Y}^k = k = 1, \ldots, K \text{ generated simultaneously on the polar calculation grid } \Gamma \quad (1c)$$

$\Re^{CALM}$ is the operator generating the radiological trajectories in STAGE I and STAGE II.

The number K from Eq. (1c) can be quite large. In our case, it represents the possible (radiological) output generated on the polar computational grid consisting of 42 concentric circles up to 100 kms from the pollution source and of 80 angular beams, numbered clockwise from North. The output matrices in (1c) thus have $80 \times 42 = 3{,}30$ entries, see Fig. 1. Examples of the various fields are:

- radioactivity concentrations of radionuclides in the air and the deposited radioactivity on the ground (*analysed in this article*), their time integrals;
- doses of external irradiation;
- internal irradiation from inhalation of contaminated air;
- internal irradiation from ingestion of contaminated food;
- …. and many others.

3 Generation of random trajectories of the output fields—sampling-based methods

This article considers the single output random field of the radionuclide ^{137}Cs deposited on the ground. It is evaluated on a matrix or "rose" on the polar computational grid Γ. A detailed description of the radionuclide propagation within the accidental radioactivity release of the CALM scenario (dissemination into the motionless atmosphere suddenly ensuing by wind) is given in the above-mentioned study by Pecha and Kárný (2021). The radioactivity [Bq· m^{-2}] deposited on the ground is examined during the complex CALM scenario consisting of the five-hour discharges into

Fig. 1 Polar computational grid on the map background in a vicinity of the Dukovany nuclear power plant. It consists of 42 concentric circles up to 100 kms from the source of pollution and 80 angular beams (clockwise, from North)

the motionless atmosphere immediately followed by four hours of ensuing windy transport (a more detailed description of the scenario is given in the Appendix). The index k stands here for 2-D radiological field of deposited radioactivity of ^{137}Cs on the ground evaluated in the discrete computational nodes according to Fig. 1.

Due to the excessive number of the input parameters, only those with significant effects of their fluctuations on the model output are assumed. They enter the analysis as random. The necessary reduction of the input-vector dimension to N is made according to the following scheme:

$$\begin{aligned} \mathbf{Y} = \Re^{\mathrm{CALM}}(\mathrm{X}_1, \mathrm{X}_2, \ldots \mathrm{X}_\mathrm{N}, \mathrm{X}_{\mathrm{N}+1}, \mathrm{X}_{\mathrm{N}+2}, \ldots) \rightarrow \\ \rightarrow \mathbf{Y} = \Re^{\mathrm{CALM}}(\mathrm{X}_1, \mathrm{X}_2, \ldots \mathrm{X}_\mathrm{N}; \mathrm{x}^{\mathrm{b}}_{\mathrm{N}+1}, \mathrm{x}^{\mathrm{b}}_{\mathrm{N}+2}, \ldots) \end{aligned} \tag{2}$$

where x^b stands for best estimated (nominal) values fixed during experiments. The assumed $\mathbf{Y}$ is ^{137}Cs deposited on the ground in nodes of the computational grid Γ, denoted by $(\mathbf{Y}^{137})_\Gamma$.

The sampling-based procedure used as a basic mathematical tool for UA and SA (both are described in Sect. 4) needs: (1) the definition of probability distributions D_i, $i = 1, \ldots,N$ characterising the uncertainty of inputs, (2) generators of input samples to be used by the uncertainty analysis, (3) the operator $\Re^{\mathrm{CALM}}$, see (1), propagating the sampled inputs, (4) a presentation of the uncertainty analysis results, and (5) evaluation of the sensitivity analysis results.

This evaluation procedure calculates the output for each sample of the random input vector. It:

generates a particular j-th sample of the input vector $\mathbf{x}^j \equiv \{x_1{}^j, x_2{}^j, \ldots, x_N{}^j\}$ where $x_i{}^j$ are realisations of the input random parameter X^j (successively, for j = 1,2,…,NREAL).

propagates the j-th input sample through the model $\Re^{\mathrm{CALM}}$ and gets the corresponding realisation $\mathbf{y}^j{}_\Gamma$ of the random output value $\mathbf{Y}$ by running the model.

$\mathbf{y}^j{}_\Gamma = \Re^{\mathrm{CALM}}(x_1{}^j, x_2{}^j, \ldots, x_N{}^j$, nominal values according to (2)).

It results in the mapping of pairs:

$$\left[\mathbf{y}^{\mathbf{j}}_\Gamma, \mathbf{x}^{\mathbf{j}}\right], \quad \mathrm{j} = 1, \ldots, \mathrm{NREAL}. \tag{3}$$

The data in (3) represents the key material for uncertainty analysis and sensitivity studies. Statistical processing of the pairs (3) can estimate the extent of the uncertainty of the predicted consequences for uncertain inputs. The simulated uncertainty propagation through the model bears cardinal importance for introduction of advanced methods in modelling; namely:

it offers essential data for transition from a deterministic procedure of the consequence assessment to the probabilistic approach, which enables us to generate more informative probabilistic answers to assessment questions,

it provides a detailed analysis of the model error covariance structure, making it possible to improve the reliability of model predictions via advanced statistical techniques of assimilation of mathematical prognoses with real measurements incoming from the terrain.

4 Uncertainty and sensitivity analysis procedures

The pairs given schematically by (3) provide the common basis for:

- *Uncertainty analysis (UA)* which provides the statistical processing of the pairs (3), quantifies uncertainties, and determines the extent of the uncertainty in the predicted consequences of the radioactive pollution. Uncertainty analyses involve the propagation of uncertainty in model parameters and model structure to obtain confidence statements for the estimate of risk and to identify the model components of dominant importance. It yields various descriptive statistics, such as the sample mean and variance, percentiles of the uncertain quantity distribution, uncertainty factors, reference uncertainty coefficients, etc.
- *Sensitivity analysis (SA)* which determines how different values of an independent input variable affect a particular output variable. It quantifies the relative impact of various sources of uncertainty on the output variables of interest, allowing decision-makers to assess the utility of further investment into uncertainty reduction. Its realisation strategies depend on the problem setting. A comprehensive outstanding study of the SA basis is presented in Saltelli et al. (2001). Many authors use the term "sensitive" when referring to the degree to which an input parameter affects the model output. The basic methods include, e.g., the differential sensitivity analysis, one-at-a-time sensitivity measures, a factorial design, sensitivity and importance indices, importance factors or subjective sensitivity analysis. Random sampling methods outlined above play a significant role in providing scatter plots, importance indices, relative deviation ratios, correlation coefficients, rank transformations or various regression techniques that are often used to replace a highly complex model by a simplified "respond surface".

Roughly speaking, the uncertainty analysis quantifies the variation in the model output, while the sensitivity analysis identifies the input sources potentially responsible for this uncertainty. UA is thus not the same as SA, but, ideally, both analyses should be run in tandem (CC-MOD

2020, Eur. Commission). A survey of sampling-based methods for calculations of the joint UA-SA analysis is reviewed in Helton et al. (2006). UA and global SA often use similar mathematical techniques based on data pairs (3). A close relation of SA with UA of numerical models is emphasised in Pianosi et al. (2016). The propagation of uncertainty by the discussed Monte Carlo simulation is also used to initialise the sampling-based sensitivity analysis. SA can address miscellaneous questions, e.g., what input factors cause the largest variation in the output, what factors are negligible or whether some factors can amplify or dampen the output variability (Pianosi et al. 2016). UA is recommended to precede SA.

There are two main ways of analysing the sensitivity:

- Local SA confronts the output variability against variations of an input around a specific, supposedly the best, estimated value x^{best} (or $\bar{x}$). The derivatives are taken at a single point and the impact of one parameter at a time is analysed while keeping the other parameters fixed. Local SA investigates the effect of variations of uncertain inputs from a baseline point. The sensitivity measure S_i for the i-th input is defined

$$S_i(\bar{x}) = \left.\frac{\partial g}{\partial x_i}\right|_{\bar{x}} \cdot c_i, \quad c_i \text{ is a scaling factor, } i = 1, \ldots, \mathrm{N}. \tag{4}$$

  The formal function g is realised by the CALM model $\Re^{CALM}$. The partial derivatives are usually approximated by finite differences. The test of local sensitivity examines the output changes when each parameter is individually increased by a factor of its standard deviation (±SD).
- Global sensitivity analysis (GSA) uses Monte Carlo sampling. GSA investigates the effects of variation of certain inputs across their entire variability space. It naturally copes with nonlinear relationships of the CALM scenario. The GSA methods are discussed in Sarrazin et al. (2016). An important technique is the Variance-Based SA method, which decomposes the observed variance. Elementary Effect Test (or method of Morris) improves the performance when the computing time of a single model run is high, or when the number of factors is very large. Regional Sensitivity Analysis, also called Monte Carlo filtering, is mentioned in Pianosi et al. (2016) as a family of methods mainly aimed at identifying regions in the input space corresponding to particular output values, say, high or low. It is used for mapping and dominant control analysis.

In Hamby (1994), the fundamental SA techniques are overviewed for the various modelling situations. A profound knowledge on SA can be gained in the principal publication by Saltelli et al. (2001). Recent trends (the most recent decade) in the sensitivity analysis practice are outlined in Ferretti et al. (2016). Sensitivity analysis of environmental models is addressed in Sarrazin et al. (2016). It inspects the sample size NREAL and the threshold for the identification of non-influential input factors. A full decomposition of the dependent-output variance is introduced in Saltelli et al. (2010).

5 On the choice of the sensitivity analysis method

The most common constraints influencing SA technique are connected with the computational expenses, the completeness of the input random parameters space, correlated inputs, nonlinearities, and the model interactions when inspecting simultaneous-inputs effects or the complexity connected with the multiple outputs. The quality of the dispersion code itself used for analysis in STAGE II can notably impact the precision.[1] A critical evaluation of the simplified solution based on the atmospheric stability characterization using the Pasquill method is given in Kahl and Chapman (2018). A number of sensitivity analysis techniques are reviewed by Hamby (1994). The simplest one-at-a-time method varies each parameter while others are fixed. Further sensitivity analysis techniques examine parameter influence based on output variations while jointly changing input parameters. It enables us to build the response surface that approximates a complex model.

Concerning the fundamental research related to the introduction and utilisation of the random sampling methods, the following reviews are important. Razavi and Gupta (2015) revisit the theoretical basis for SA, critically evaluate existing approaches in the literature and demonstrate their flaws and shortcomings through the published examples. They identify important properties of SA associated with the interpretation of sensitivity in context of Earth and Environmental-systems models. A systematic review of sensitivity analysis practice is made by Saltelli et al. (2019). A question "Why so many published sensitivity analyses are false?" is opened. Many published SA instances fail the elementary requirement to properly explore the space of the input random factors. Warning before perfunctory settings of the sensitivity scenario is emphasised in Saltelli (2010). One should be aware of

[1] As said in the Introduction, the used algorithm for a Gaussian puff model, Adriaensen (2002), with the plume-segmented modification, was selected here for demonstration purposes only. In reality, more sophisticated dispersion codes are assumed to be applied. Their complexity and computational load could be diminished by the positive effect of the approximation-based (*AB*) procedure.

pitfalls and avoid the false procedures. Saltelli and Annoni (2010) warn that conclusions drawn from GSA should be taken with care when the input variability space is poorly known.

Even with these drawbacks, GSA gradually replaces traditional local techniques of sensitivity analysis, Ferretti et al. (2016). Especially, when sensitivity indices cannot be computed analytically, sampling-based sensitivity analysis must be used. Typically, the number of model evaluations NREAL increases with the number of input factors N subject to SA. However, the ratio between NREAL and N significantly varies from one method to another and often also from one application to another. The combinations (NREAL, N) are usually taken as a compromise between the environmental model computational complexity and completeness of the input parameter uncertainty group. In this context, the possibility to explore input-parameter space more thoroughly, offered by *AB*, is quite significant.

6 Setting up the CALM scenario of radioactive discharges

We focus on the near-field analysis below the mixing layer in a small spatial domain up to 100 km from the source of pollution. The inspected area is shown in Fig. 1. A more detailed explanation of the analysed CALM scenario is given in the Appendix.

7 Definition of the specific uncertainty group of the atmospheric dispersion and deposition model of the CALM scenario

The input random parameters X can be split in two alternatives forms:

$$\text{Fractional}: \quad X = f * x^{best}; \quad \text{Additive}: \quad X = x^{best} + \Delta f \tag{5}$$

The fraction f or the shift Δf are random numbers with a suitable probabilistic distribution, x^{best} is the best estimate (reference, nominal) of the input value, see panels for LHS sampling below. As said above, the release scenario consists of STAGE I and STAGE II. The accidental release of radioactive substances into the motionless (calm) atmosphere is followed by the radioactivity dissemination into the living environment caused by the wind. Similarly, the uncertainty group differs for the calm region and for the convective transport.

Input parameters selected as random for atmospheric dispersion model in the CALM region:

ADMXX(1) …. random fraction for horizontal dispersion parameter $^{CALM}\sigma_y$.
ADMXX(2) …. random fraction for vertical dispersion parameter $^{CALM}\sigma_z$.
ADMXX(3) …. absolute random value for gravitational settling velocity in the calm region—in LHS sampled from absolute interval—see Panel LHS Part I.
ADMXX(4) …. random fraction for scavenging coefficient for aerosol.

Following the more detailed description in Appendix, after 5 h of the calm, the motionless atmosphere is dispersed by the wind into the surrounding environment. The radioactivity package accumulated locally during the last 5 h is immediately drifted onward. We assume 4 h of the successive convective transport. In the 4th hour, the atmospheric precipitation with intensity 1 [mm·h^{-1}] occurs.

Input parameters selected as random for atmospheric dispersion model—continuation for the convective stage of the CALM scenario:

ADMXX(5) …. random fraction for horizontal dispersion parameter CONVσy: *KFK-Jűlich formulae*, see e.g. Kahl and Chapman (2018).
ADMXX(6) …. random fraction for vertical dispersion parameter CONVσz: *KFK-Jűlich formulae*
ADMXX(7) …. random fraction of dry deposition velocity vg for aerosol ADMXX(8) …. random fraction for scavenging (washout) coefficient Λ for aerosol
ADMXX(9) …. random fraction of the wind direction fluctuations added to the best estimated value for p = 1: the 1st hour of convective transport ADMXX(10) …. random fraction for wind speed fluctuations.
for p = 1: the 1st hour of the convective transport.
ADMXX(11)…..same as ADMXX(9) for p = 2: the 2nd hour of the convective transport.
ADMXX(12)…..same as ADMXX(10) for p = 2: the 2nd hour of the convective transport.
ADMXX(13)…..same as ADMXX(9) for p = 3: the 3nd hour of the convective transport.
ADMXX(14)…..same as ADMXX(10) for p = 3: the 3nd hour of the convective transport.
ADMXX(15)…..same as ADMXX(9) for p = 4: the 4nd hour of the convective transport.
ADMXX(16)…..same as ADMXX(10) for p = 4: the 4nd hour of the convective transport.

Two software subsystems have been developed for: (i) multiple generation of the samples from the input model parameters, and (ii) visualization of 2-D results, cf. Section 3. They are:

1. *Latin hyperculbe sampling (LHS) generation subsystem:* random characteristics of the input parameters are

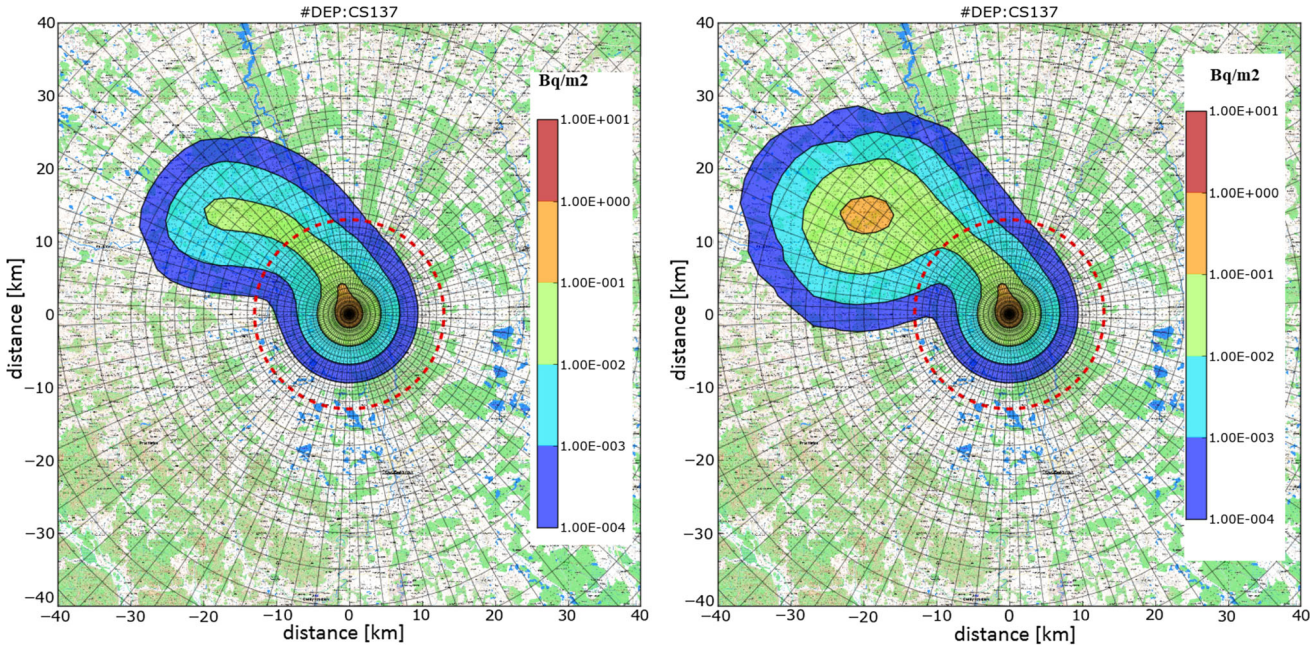

Fig. 2: 2-D radiological trajectories for the nominal (best estimate) input values. It shows the deposition of radionuclide ^{137}Cs on terrain [Bq.m^{-2}], the detailed image of the deposition for the CALM scenario just after 5 h of the calm episode plus 4 h of the successive convective transport. Left: No atmospheric precipitation; Right: Hot spot of the deposited radioactivity induced by the rain of intensity 1 [mm.h^{-1}] within the 4th (last) hour of the convective transport

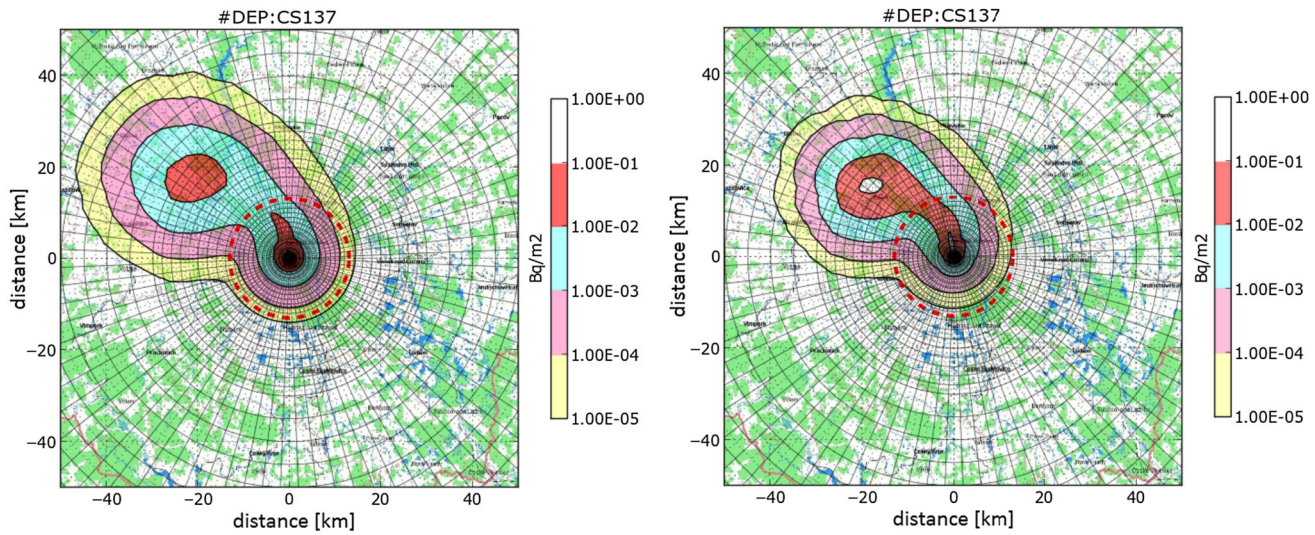

Fig. 3 NRE = 2 (left), NRE = 3 (right)

specified and recorded to PANELs LHS (see below). More detailed options are shown on the example of the detailed random characteristics entering ADMXX(7) from Panel LHS Part I.

2. *Special graphical subsystem for visualization:* the resulting output-dependent fields, see Eq. (2), are drawn as 2-D pictures—see Figures 2 and 3.

The adopted Monte Carlo modelling is integrated into the CALM scenario. It uses the stratified sampling procedure LHS (see LHS Panel below). The generation of NREAL samples continues from the various types of random distributions D_n of the random vector inputs X_n (n = 1, …, N). A technique for correlation control between inputs X_n can be included. The LHS tends to produce more stable results than the common random generators.

Detailed options of the input parameters of the atmospheric and deposition model and its random characteristics are given in the following Panel LHS Part I Scenario CALM.

Panel LHS Part I Scenario CALM: Generating NREAL = 5000 realisations of 16 random input atmospheric dispersion parameters. Potential correlation settings: ADM1 x ADM2; ADM5 x ADM6.

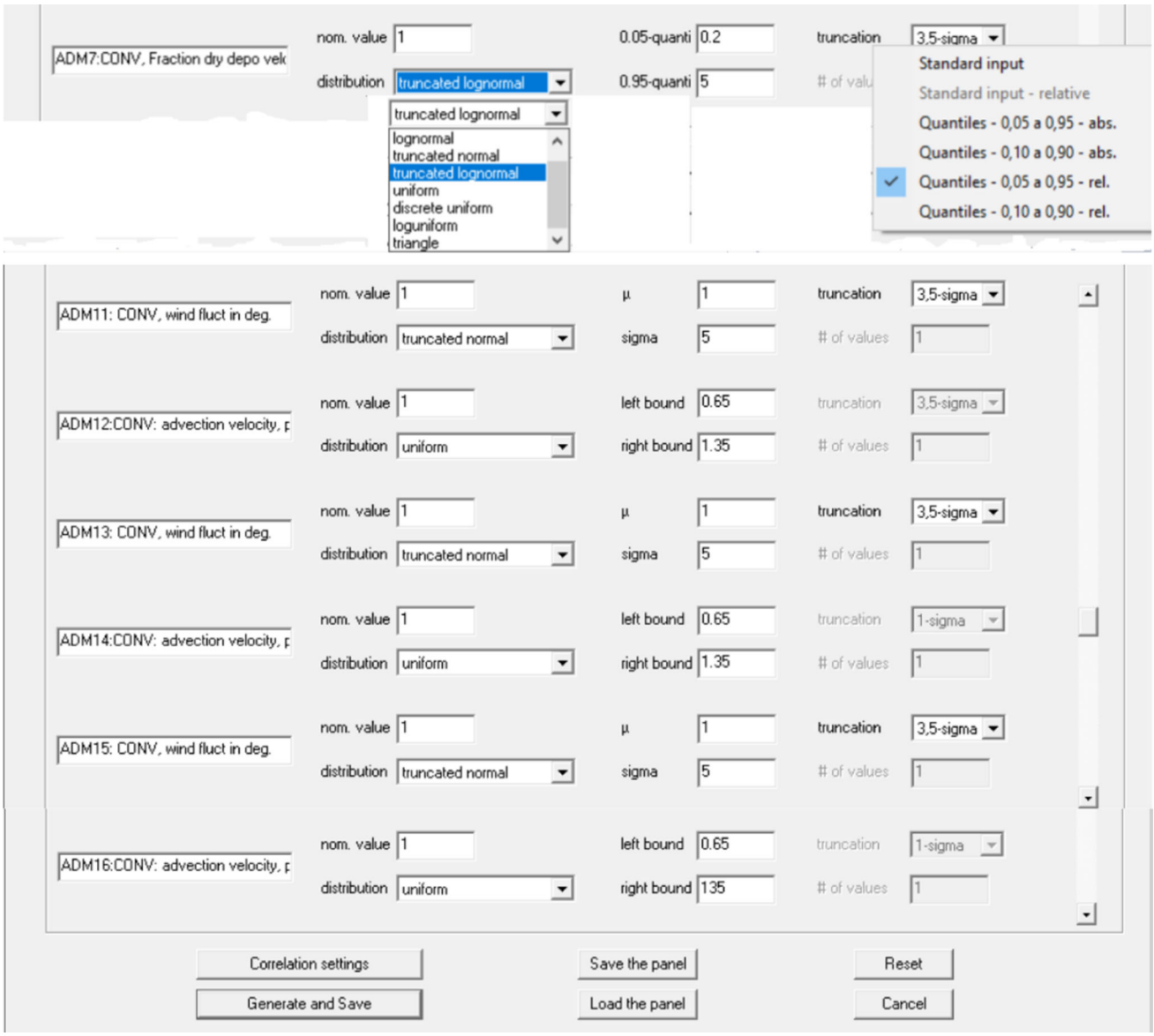

Example of a detailed selection ADMXX(7): Panel LHS Part I Scenario CALM—continuation: Scenario CALM: Generating NREAL = 5000 realisations of 16 random input atmospheric dispersion parameters.

A special attention is paid to critical areas. The space of random inputs should be properly explored with respect to their completeness.[2] Some inputs can be strongly correlated or the model responses can be nonlinear with respect to their inputs. Setting of the group of random inputs, given on the Panels pictures above, come from the former international codes COSYMA, UFOMOD, MARC-2 and others analyses. The data were collected and used in Pecha and Pechova (2005). Quality of the input parameter

[2] Someone may object why the input parameter of the total inventory of radionuclide was not considered as random. This factor is assumed to enter separately at a higher level procedure of inverse modelling for estimation of the source term. The problem was addressed, e.g. in Pecha and Šmídl (2016), and requires real measurements from the monitoring networks.

uncertainty group should be actualised of basis of the new knowledge elicitation procedures.

8 Results for UA and SA of the accidental scenario CALM

The near-field dispersion and deposition of radioactive mixtures below the mixing layer in a small spatial domain up to 100 km from the source of pollution are examined, Fig. 1. STAGE I and STAGE II of the numerical experiment are designed (consult the text above and Appendix) for a hypothetical release from the category of the worst-case analysis of Weather Variability Assessment. In the first five hours of the STAGE I, the release dissipates into the motionless ambient atmosphere just until the calm-period termination. When the calm condition ends, immediately the second convective phase STAGE II of the transport induced by the wind starts. The hourly wind speeds and directions, rain episodes, atmospheric stability classes are provided by the regional meteorological service.

8.1 UA results

A part of results is illustrated by 2-D radiological trajectories. The values calculated for the best estimate of input parameters are shown in Fig. 2. A more detailed presentation is in Pecha et al. (2020).

UA analysis uses pairs [$\mathbf{y}^{j}_{\Gamma}$;$\mathbf{x}^{j}$] given by the pattern according to Eq. (3). The influence of the random-inputs realisations is shown on Figs. 3, 4, 5, 6, 7. The ordinal number of the random realisation of the vector $\mathbf{x}^{j}$ is marked as NRE. The pictures of $\mathbf{y}^{j}_{\Gamma}$ stands for several selected realisations NRE from the whole range of NRE $\in$ < 1; NREAL >). The complex random 2-D radiological trajectories are valid for the CALM scenario with 5 h of radioactivity release into the motionless atmosphere immediately succeeded by 4 h of the convective windy transport (with the rain 1 [mm.h^{-1}] in the 4th (last) hour of the convective transport). In other words, the pictures are "snapshots" of the ^{137}Cs deposition (labelled as #DEP:CS137) on the ground at to the beginning of the 10th hour after the release start.

8.2 Comments on SA results: sensitivity analysis utilising random sampling method

The input parameters whose uncertainty makes a major contribution to the overall uncertainty can be identified using the correlation coefficients PRCCs, PCCs and SRCs, e.g., Saltelli et al. (2001). The identification of important contributors to the variations of consequences is done using so-called partial (rank) correlation coefficient. It is possible to calculate the percentage contribution of each uncertain model parameter to uncertainty of consequences by use of so-called coefficients of determination (R^2). The simplest type of SA perturbs the input factors entering the model g, Eq. (4), from their nominal values one at a time. The measure of output sensitivity to the i-th input factor is based on the partial derivative of the dependent value at the nominal values of other factors k $\neq$ i, see Eq. (4). Many other tests with different degrees of complexity are outlined in Humby (1994).

The most common sensitivity analysis uses sampling. The model runs repeatedly for a combination of input-factor values from the respective distributions. Sampling-based methods do not require access to model equations: they (may) work with a software model. They benefit from

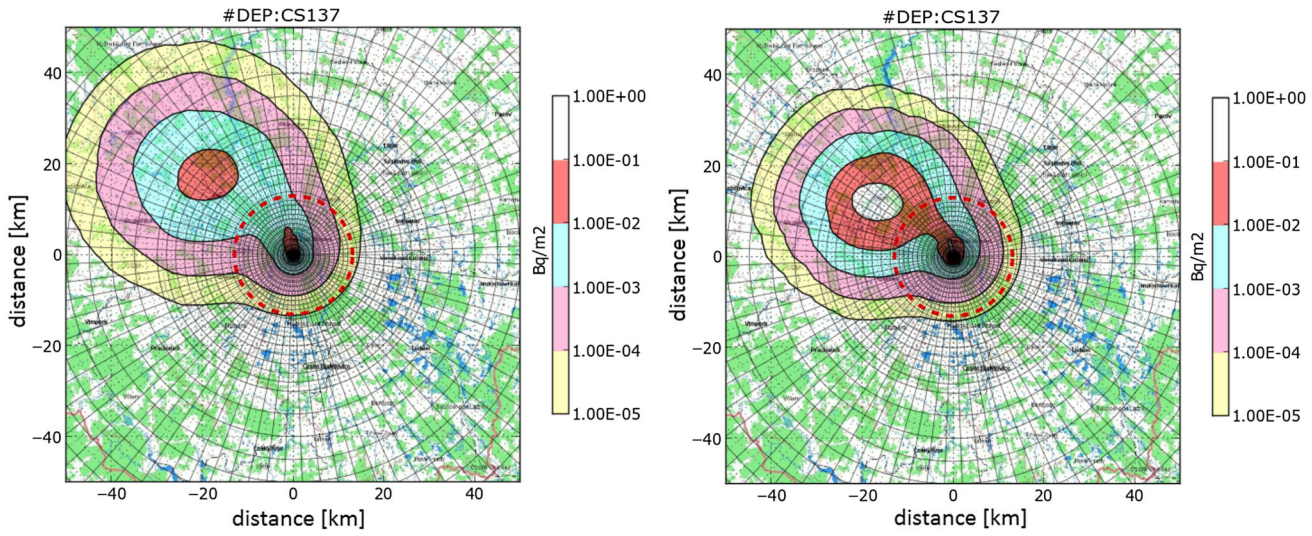

Fig. 4 NRE = 4 (left), NRE = 5 (right)

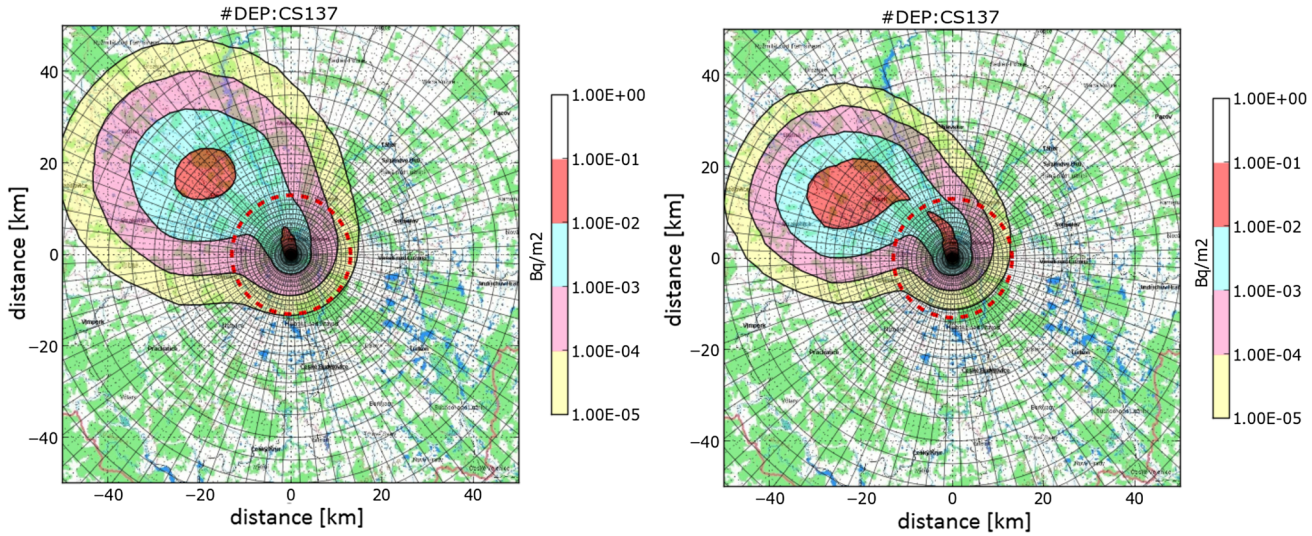

Fig. 5 NRE = 6 (left), NRE = 9 (right)

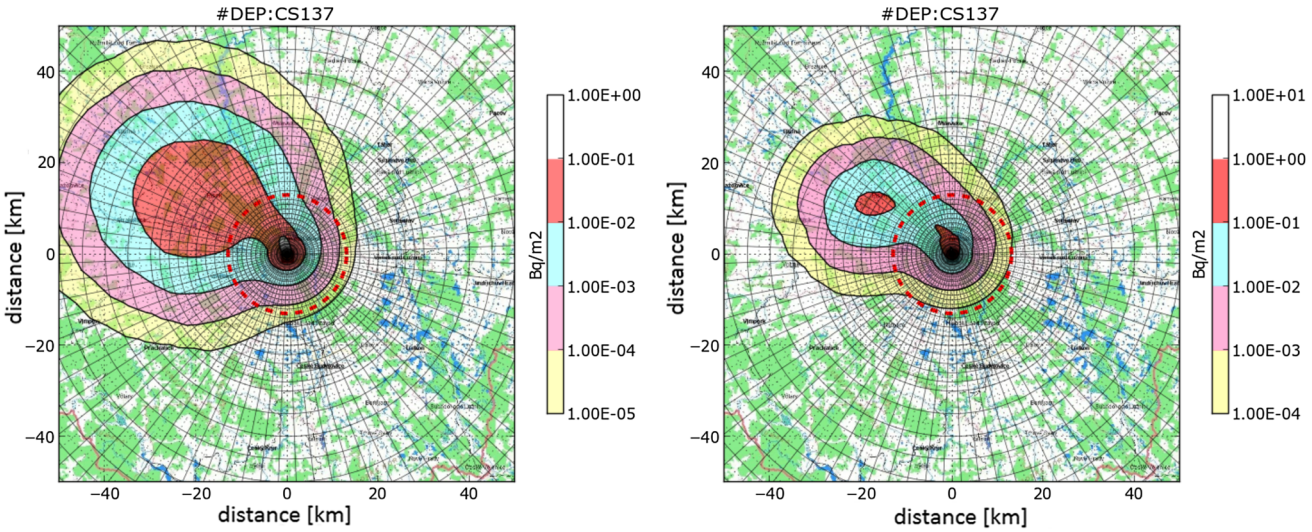

Fig. 6 NRE = 12 (left), NRE = 13 (right)

our research substantially enhancing feasibility of the global SA. The main problem of SA concerns the computational cost of the analysis brought the high number of evaluations of the environmental-model response in the CALM scenario. The number should guarantee that the sensitivity estimates are independent of the size of the processed input–output sample. The problem may appear even if the number of samples is of a medium size. The dependence of the robustness and convergence of the CALM scenario on the sample size becomes much less critical due to the substantial acceleration brought by the *AB* procedure.

Let us recall that the dependent output values are arranged into the matrix consisted from $N^{\Gamma} = 3360$ elements (42 concentric circles × 80 angular beams). N^{Γ} is the dimension of the output vector field on the computational grid Γ. We shall a bit simplify by focusing our considerations on Eq. (1a) for a single point *node* on Γ in the form:

$$y^{Cs137}\left(node, \mathbf{x}^{k}\right)_{node\in\Gamma} = y_{k}^{node} \tag{6}$$

y_k^{node} represents the deposition of ^{137}Cs on the ground exactly in the discrete spatial point *node* of the calculation polar grid Γ (Fig. 1) for the k-th realisation $\mathbf{x}^k \equiv \{x_1^k, x_2^k, \ldots x_N^k\}$ of the input random vector $\mathbf{X}$. As stated above, the sampling-based methods for UA consist of NREAL repetitions of output calculations, successively for each specific sample of random input vector. The sensitivity evaluation itself can be done at any point of the spatial computational grid. Various techniques can be used providing different

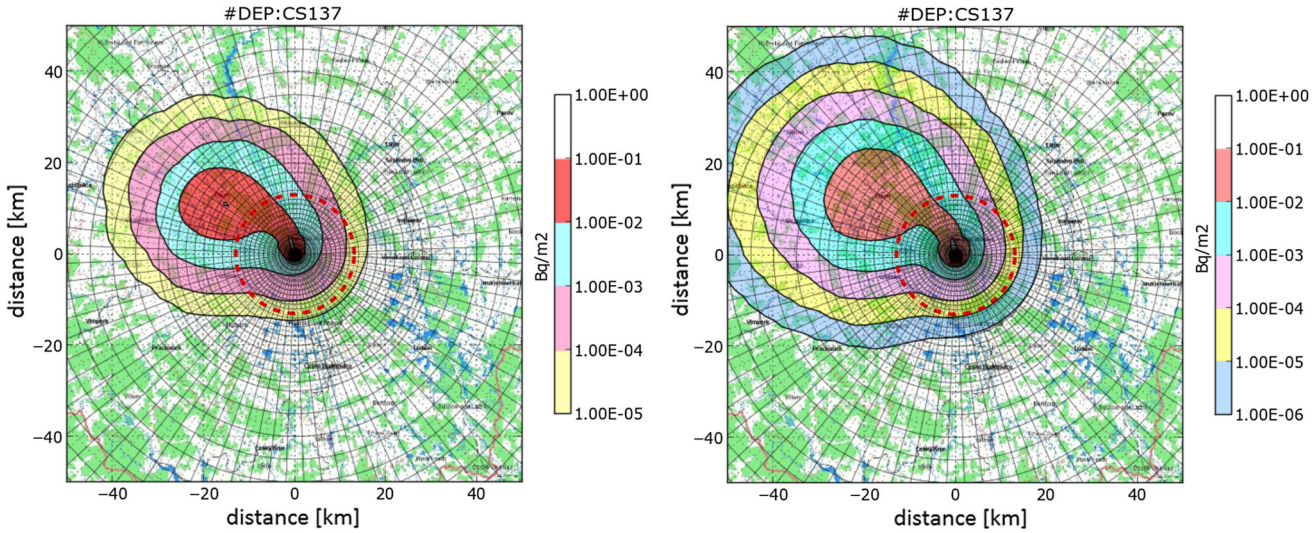

Fig. 7 NRE = 15 (left); Sum of all $\mathbf{y}^{j}_{\Gamma,}$ j = 1, …,NREAL,given by Eq. (3) averaged for NREAL = 1000, (right)

measures of sensitivity (scatterplots, regression and correlation analysis, rank transformations etc.). As a demonstration example we shall outline determination of the Pearson correlation coefficient c(x_j, y; *node*). It expresses a measure of strength of the linear relationship between x_j and y at a computational point *node*. It has the form:

$$c\left(x_j, y\,; node\right) = \frac{\sum_{k=1}^{NREAL}\left(x_j^k - \bar{x}_j\right)\,.\,\left(y_k^{node} - \bar{y}^{node}\right)}{\left[\sum_{k=1}^{k=NREAL}\left(x_j^k - \bar{x}_j\right)^2\right]^{1/2}\cdot\left[\sum_{k=1}^{k=NREAL}\left(y_k^{node} - \bar{y}^{node}\right)^2\right]^{1/2}} \tag{7}$$

$$\begin{aligned}\bar{x}_j &= \sum_{k=1}^{NREAL} x_j^k\ /NREAL\,; \qquad \bar{y}^{node} \\ &= \sum_{k=1}^{NREAL} y_k^{node}\ /NREAL\,;\end{aligned} \tag{8}$$

The larger the absolute value of *c(x_j, y; node)* is, the stronger degree of linear relationship between the input and output values is. The numerical results are assigned to selected grid points. These points, labelled as **node** = 1; **node** = 17; **node** = 20; **node** = 25, are marked in Fig. 8. All are laying on the angular beam b = 69 (around the maximum nominal values). **Node = 25** is laying inside the rainy 4th convective phase.

Even in the simplified case of this point-based SA, some considerations have to be added. It turned out to be necessary to discriminate the nature of the action of the random input parameters x_j as local or global. For example, from this point of view, the input random factors ADMXX(1), ADMXX(2), ADMXX(3) and ADMXX(4) are assumed to act independently inside the calm region. On the other hand, the random inputs factors in the convective region can impact the convective region either globally (same in all phases) or locally (independently in each convective phase: the precipitation, the speed and direction of the wind are available for each hour of propagation). The sample-based technique leading to Eq. (3) can naturally comply with the local or global character impact of random input parameters. Finally, some inputs are correlated mutually. Specifically, the horizontal dispersion in the convective region is evaluated according to the expression (4.2) in Pecha and Kárný (2021). In hourly phase p along the total convective transport length L_p, it is expressed by sum:

$$\sigma\left(L_p + l\right) \;=\; \sigma(T_{END}^{CALM}) + \;\Delta\sigma\left(L_p + l\right) \tag{9}$$

The first addend stands for dispersion of the puff m from its birth at t_m until $t = T_{END}^{CALM}$. Randomisation is expressed consistently according to the random scale factor ADMXX(1). The second addend $\Delta\sigma\left(\,L_p\,+l\,\right)$ is the contribution to the dispersion along the total convective transport length $L_p + l$. The responsible random scale factor ADMXX(5) is assumed to act locally (independently in each hourly phase p). We can hardly anticipate the correlations of such composite variables.

9 Selected numerical results

We have focused on dependent variable of the radioactivity deposition on the ground. In STAGE I (calm region) we assume unchanged meteorological conditions (global character of uncertainties—unchanged values of the parameters during the whole period $\langle T_{START}^{CALM};\ T_{END}^{CALM}\rangle$). Unlike this, in the convective STAGE II some uncertainties can have local character of their effect. For example, dry deposition velocity v_g depends on the land-use

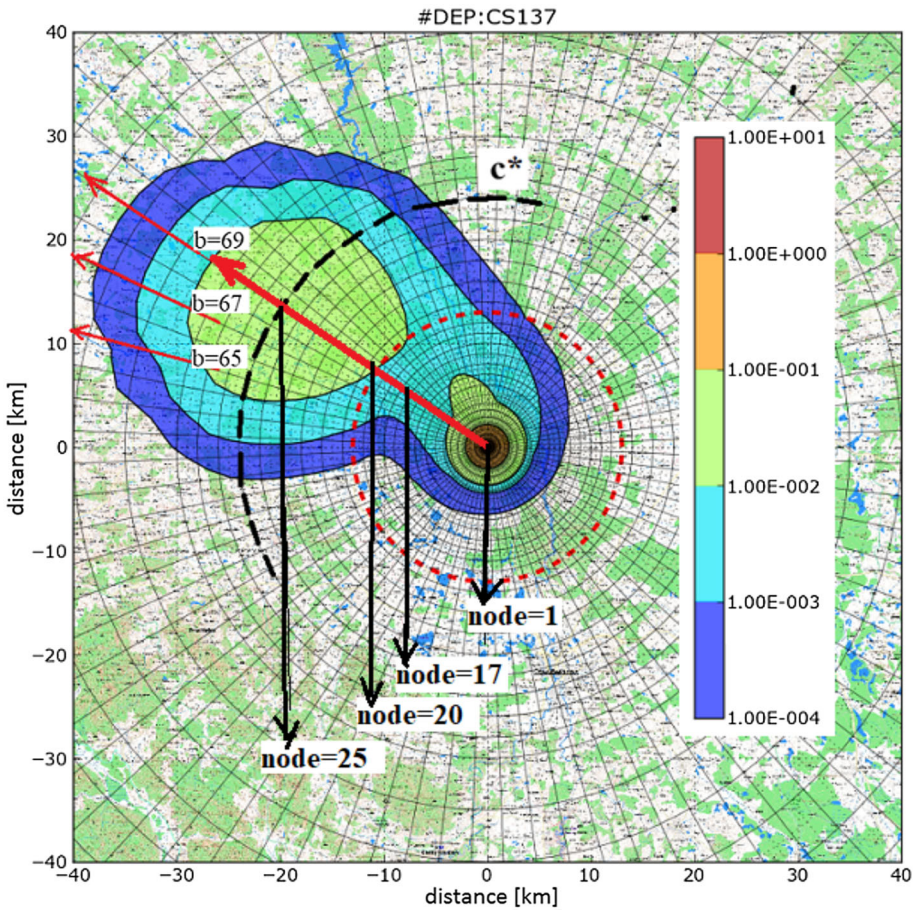

Fig. 8 "Hot spots" of deposited radionuclide ^{137}Cs on the terrain. The radioactivity release is split into $M = 100$ *of* discrete radioactivity pulses, *BF* solution, serrated release source strength. Atmospheric precipitation occurs with intensity *1.0* $[mm.h^{-1}]$ in the 4th hour of the convective transport. Red arrow stands for the selected for correlation calculations: angular beam no. 69 with four **nodes** = 1; 17; 20; 25 (radius = 0; 10.5 km; 15 km; 25 km from the source)

characteristics in a specific phase *p*. Similarly, the atmospheric precipitation in a particular phase p can be zero or non-zero. So, inputs x_7 and x_8, given below, can have a local character. The coefficients (7) for respective nodes are:

node = 1 ⇔ the centre of the calm region:

x_1 = ADMXX(1) …. $^{CALM}\sigma_y$; horizontal dispersion $c(x_1, y; node = 1) = -$ 1.59E-01.

x_2 = ADMXX(2) …. $^{CALM}\sigma_z$; vertical dispersion $c(x_2, y; node = 1) = -$ 2.31E-01.

x_3 = ADMXX(3) …. gravitational settling velocity v_{grav}. for aerosol $c(x_3, y; node = 1)$ = 4.70E-01.

x_4 = ADMXX(4) …. scavenging coefficient. for aerosol $c(x_4, y; node = 1)$ = 4.86E-02 *

* not relevant (no rain in the calm region).

Findings for node = 1: the strong negative correlation between dispersions and deposited activity on the ground and the strong positive correlations with the gravitational settling velocity are expected.

node = 17 ⇔ the convective region on the beam $b = 69$, Fig. 8, 10.5 [km], the convective phase $p = 2$:

x_7 = ADMXX(7) …. dry depo. velocity v_g for aerosol $c(x_7, y; node = 17)$ = 4.62E-01 x_8 = ADMXX(8) …. scavenging coefficient for aerosol $c(x_8, y; node = 17)$ = 4.86E-02 ** x_{11} = ADMXX(11) wind direction fluctuations, additive to the best estimation value, see (5), the 2nd hour of convective transport $c(x_3, y; node = 1)$ = 4.70E-01.

x_{12} = ADMXX(12) ….wind speed fluctuations, the 2nd hour of the convective transport.

$c(x_{12}, y; node = 17)$ = -4.47E-01.

** not relevant (no rain in the phase 2).

Findings for node = 17: the strong positive correlation between dry deposition, velocity v_g for aerosol and deposited activity on the ground as well as negative

correlations with wind direction and wind speed fluctuations are expected.

node = 20 ⇔ the convective region on the beam b = 69, Fig. 8, 15 [km], the convective phase p = 3:

x_7 = ADMXX(7) …. dry depo. velocity v_g for aerosol $c(x_7,\ y;\ node = 20)$ = 1.31E-01 x_8 = ADMXX(8) …. scavenging coeff. for aerosol $c(x_8,\ y;\ node = 20)$ = 3.60E-01 *** x_{13} = ADMXX(13) …wind direction fluctuations, additive to the best estimation value, see (5), the 3rd hour of convective transport $c(x_{13},\ y;\ node = 20)$ = -8.66E-02.

x_{14} = ADMXX(14) ….wind speed fluctuations, the 3rd hour of convective transport.

$c(x_{14},\ y;\ node = 20)$ = -3.24E-01.

*** not relevant (no rain in the phase 3).

Finding for node = 20: they are identical with those for the node = 17.

node = 25 ⇔ the convective region on the beam b = 69, Fig. 8, 25 [km], the convective phase p = 4, precipitation 1 [$mm.h^{-1}$]:

x_7 = ADMXX(7) …. dry depo. velocity v_g for aerosol $c(x_7,\ y;\ node = 25)$ = -7.32E-03 x_8 = ADMXX(8) …. scavenging coefficient for aerosol $c(x_8,\ y;\ node = 25)$ = 6.66E-01.

x_{15} = ADMXX(15) wind direction fluctuations, additive to the best estimation value, see (5), the 4th hour of convective transport $c(x_{15},\ y;\ node = 25)$ = 1.86E-02.

x_{16} = ADMXX(16) ….wind speed fluctuations, the 4th hour of convective transport.

$c(x_{16},\ y;\ node = 25)$ = -1.04E-01.

Findings for node = 25: a strong positive correlation between precipitation intensity and deposited activity on the ground prevails.

10 Conclusions

The uncertainty analysis of the CALM release scenario is based on data pairs, see Eq. (3). The sensitivity analysis comes out of the same source. Its quality directly depends on the degree of the inspected details. The UA can inherently include global or local character of the random input parameters. The latter may exhibit same or differing fluctuations in separate spatial regions. UA can account for correlations of inputs. The more detailed the UA is, the more sophisticated SA can be accomplished. The analysis is, however, constrained as discussed in Sect. 5. The constraints concern the completeness of the uncertainty group of the random input parameters, the insufficient description of the real physical processes for the used parameterisation, the incomplete knowledge of sub-model parameters, the uncertain release scenario, the consequences of simplifications of the used computational procedures, etc.

The demonstrated point-based SA is useful for the fast and effective estimation of the sensitivity measures in different computational nodes. Positive correlations between random scaling factors of the input parameters of the deposition processes (gravitational settling, dry velocity deposition, washout from the plume by rain) and the inspected dependent random variable y (here the ^{137}Cs radioactivity deposition on the ground) have been confirmed. At the same time, the negative correlations for input parameters ADMXX(1) ($^{CALM}\sigma_y$—horizontal dispersion) and ADMXX(2) ($^{CALM}\sigma_z$—vertical dispersion) comply with the local character of their effects limited to the calm region only.

The significantly sped-up evaluations were achieved by an original, well-justifiable approximation of the final non-Gaussian superposition of the Gaussian puffs by a single Gaussian "super-puff". The concept of this *AB* procedure is described in the Introduction. This article demonstrates its functionality and shows the advantages on the overall uncertainty and sensitivity analysis for the calm scenario. Substantial benefits can be gained for the calm scenario analysis exploiting computationally-intensive Monte-Carlo sampling techniques.

The assimilation methods of the measured data in the terrain using static or mobile sensors with the model predictions were studied, e.g., in Hutchinson et al. (2017). The specific application on the Chernobyl source term inversion problem is examined in Evangeliou et al. (2017). The problem of the source term reconstruction was tested during the customisation of the RODOS system for the Czech Republic. All of these problems indicate the potential use of the advocated *AB* technique.

Thanks to the *AB* approach, the UA and SA analyses for the CALM scenario are fairly feasible even for the relatively high numbers of random realisations NREAL, of input random parameters N and the number of employed puffs M. The discussed benefit can be seen on the parameter sensitivity analysis utilising the random sampling method explained in Sect. 8.2. The results for a high NREAL $> 10^3$ and the number of puffs $M \sim 100$ have been gained by the *AB* solution in the convective stage roughly M-times faster than via the *BF* calculations. On a common laptop computer, the *AB* solution with one "super-puff" run takes about tens of minutes comparing to tens of hours for the *BF* calculation.

Appendix

Demonstration of the "super-puff" concept (AB solution), see Pecha and Kárný (2021).

The CALM scenario ranks among the worst-case episodes of Weather Variability Assessment. Let total

Table 1 Convective transport in the subsequent four hours (immediate continuation of the calm episode). Archived meteorological data at point (49° 05′ 00.73″ N, 16° 07′ 26.95″ E) of the Dukovany nuclear power plant: start at Dec 4, 2019, 01.00 CET (time_stamp 2,019,120,401). Rain in the 4th convective hour was chosen deliberately for demonstration purposes

time_stamp	Pasquill_cat	mean wind speed at 10 m	wind_direction	rain
yyyymmddhh	**	height [m.s^{-1}]	[°]*	[mm.h^{-1}]
……	……	……	……	……
2,019,120,401	…F…	..1.8…	345.0	0.0
2,019,120,402	…F…	..3.2…	312.0	0.0
2,019,120,403	…F…	..2.2…	280.0	0.0
2,019,120,404	…F…	..2.2…	260.0	1.0
…….	……	……	……	……

* Clockwise, from the North ** Pasquill atmospheric stability class

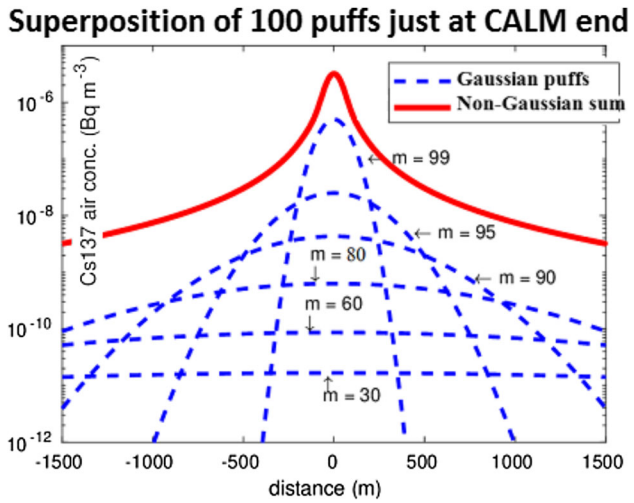

Fig. 9 Distribution of ^{137}Cs concentration in air for separate puffs m having its own age. Red line: procedures of handling the further convective superposition of all puffs m; $m \in \{1,\ldots,M\}$

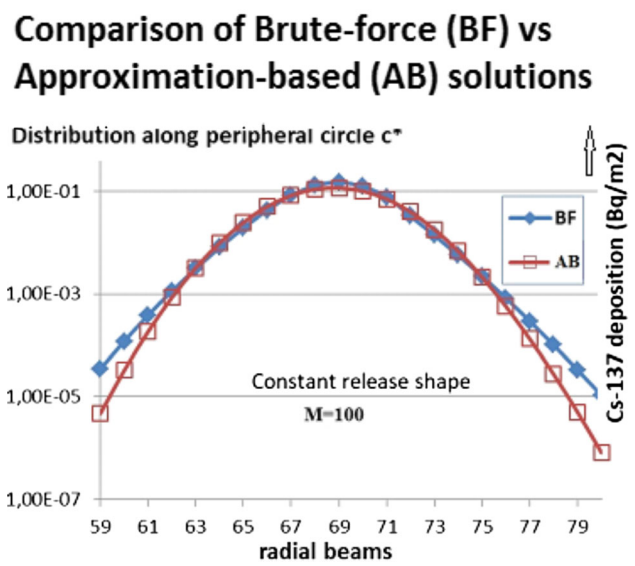

Fig. 10 Comparison of two alternative procedures of handling the further convective transport

inventory $Q^n_{TOT} = 6.0\ E + 07$ [Bq] of radionuclide ^{137}Cs be discharged into the motionless ambient air during the calm conditions lasting $T^{CALM} = 5$ [h], $T^{CALM} = \left(T^{CALM}_{END} - T^{CALM}_{START}\right)$. The release is modelled as a sequence of M instantaneous discrete discharges, the first (oldest puff) for $m = 1$ at time T^{LEAK}_{START}, the last for $m = M$ at time T^{LEAK}_{END}. The release propagates from the elevated point source of pollution at a height of H ($x = 0$; $y = 0$; $z = H$) over the terrain. The radioactivity progresses during the calm episode time interval $\langle T^{LEAK}_{START};\ T^{CALM}_{END}\rangle$. The chain of consecutive discrete puffs Q^n_m of ^{137}Cs, $m \in \{1,\ldots,M\}$, are ejected stepwise with the time periods Δt_m. The release-source strength Q^n_{TOT}/M is initially assumed to be constant within the entire calm episode. After five hours of the calm episode, the wind begins to blow. The convective transport of the radioactivity clew immediately arises. We trace the drifting over the terrain in the next four hours. Meteorological records are extracted from stepwise forecast series for the given point of radioactive release. Hourly meteorological data of the convective transport immediately following the five hour calm episode are shown in Table 1.

Each puff reflects a partial discharge of the radioactivity Q^n_m, $m \in \{1,\ldots,M\}$, which dissipates into the motionless ambient atmosphere just until to the calm-period termination. The results of current realistic calm scenario in STAGE I (related to T^{CALM}_{END}) are displayed in Fig. 9. Radioactivity concentrations of ^{137}Cs in air (in the height H) for each individual puff m are shown here. The sharpest shape for the "youngest" puff $m = 99$, the flattened shape for the "oldest" $m = 30$, has been expected. The red curve shows, clearly non-Gaussian, shape of the puffs' superposition.

The radiological results transformed into radioactivity concentration values of ^{137}Cs deposited on the ground at the end of the STAGE II (just after 9 h from the same

beginning of the CALM start) are shown in Fig. 10. It represents the peripheral distribution (around the angular beam of the computational grid containing maximum values of deposited radioactivity) on the concentric circle c^* ($\sim$ 25 [km] around the release point (of the computational grid). The results confirm a good agreement of both compared solutions in the domains of interest (with potential high values of harmful effect on the population). Several variants have been successfully tested including nonlinear releasing, serrated form, the dependency of AB approximation on the number of puffs M, etc.

Acknowledgements The authors are grateful to the IT department of the National Radiation Protection Institute in Prague for free access to the archives of the historical meteorological data. The research of MK was partially supported by MŠMT ČR LTC18075 and EU-COST Action CA1622. Dr. T.V. Guy provided us a useful feedback on the presentation way.

References

Adriaensen S, Cosemans S, Janssen L and Mensink C (2002): PC-Puff: A simple trajectory model for local scale applications. In: Berbia CA (ed) Risk analysis III. ISBN 1-85312-915-1.

Bangotra P, Sharma M, Mehra R, Jakhu R, Singh A, Gautam AS, Gautam S (2021) A systematic study of uranium retention in human organs and quantification of radiological and chemical doses from uranium ingestion. Environ Technol Innov. https://doi.org/10.1016/j.eti.2021.101360

Bernardo J (1979) Expected Information as Expected Utility. Ann Stat 7:686–690

Carruthers DJ, Weng WS, Hunt JRC, Holroyd RJ, McHugh CA and Dyster SJ (2003) PLUME/PUFF spread and mean concentration - Module specifications. ADMS4 paper P10/01S/03, P12/01S/03

ECC-MOD: Sensitivity analysis of models https://ec.europa.eu/jrc/en/samo, update 10/02/20

EPA (2004) AERMOD: Description of Model Formulation. U.S. Environmental Protection Agency, Research Triangle Park, NC (Report EPA-454/R-03–004)

Evangeliou N, Hamburger T, Cozic A, Balkanski Y, Stohl A (2017) Inverse modelling of the Chernobyl source term using atmospheric concentration and deposition measurements. Atmos Chem Phys 17(14):8805–8824

Ferretti F et al (2016) Trends in sensitivity analysis practice in the last decade. Sci Total Environ 568:666–670. https://doi.org/10.1016/j.scitotenv.2016.02.133

HARP: HAzardous Radioactivity Propagation (2010–2021) - Program system for modelling of radioactivity propagation into the living environment. https://havarrp.utia.cas.cz/harp/

Helton JC, Johnson JD, Sallabery CJ and Storlie CB (2006) Survey of sampling-based methods for uncertainty and sensitivity analysis. SANDIA report SAND2006–2901, 2006

Hershey JR, Olsen PA (2007) Approximating the Kullback Leibler divergence between Gaussian mixture models, ICASSP '07, Honolulu, HI, IV-317-IV-320

Humby DM (1994) A review of techniques for parameter sensitivity analysis of environmental models. Environ Monit Assess 32:135–154

Hutchinson M, Hyondong O, Wen-Hua C (2017) A review of source term estimation methods for atmospheric dispersion events using static or mobile sensors. Inf Fusion 36:130–148

Hyojoon J, Misun P, Wontae H, Enuhan K, Moonhee H (2013) The effect of calm conditions and wind intervals in low wind speed on atmospheric dispersion factors. Ann Nucl Energy 55:230–237

Kahl JDW, Chapman HL (2018) Atmospheric stability characterization using the Pasquill method: a critical evaluation. Atmos Environ 187:196–209

Kárný M, Guy TV (2012) On support of imperfect Bayesian participants. Decis Mak Imperfect Decis Makers. https://doi.org/10.1007/978-3-642-24647-0

Kullback S, Leibler R (1951) On information and sufficiency. Ann Math Stat 22:79–87

McLachlan GJ, Peel D (2000) Finite mixture models. Wiley, Hoboken

Pandey G, Sharan M (2019) Accountability of wind variability in AERMOD for computing concentrations in low wind conditions. Atmos Environ 202:105–116

Pecha P, Kárný M (2021) Novel simulation technique of harmful aerosol substances propagation into the motionless atmosphere suddenly disseminated by wind to surrounding environment. Ann Nucl Energy. https://doi.org/10.1016/j.anucene.2021.108686

Pecha P, Šmídl V (2016) Inverse modelling for real-time estimation of radiological consequences in the early stage of an accidental radioactivity release. J Environ Radioact 164(1):377–394

Pecha P, Tichý O, Pechová E (2021) Determination of radiological background fields designated for inverse modelling during atypical low-wind speed meteorological episode. J Atmos Environ 246:118105

Pecha P, Hofman R (2007) Integration of data assimilation subsystem into environmental model of harmful substances propagation. In: Carruthers DJ (Ed.), Proc. 11th Int Conf on Harmonisation within Atmospheric Dispersion Modelling, 111–115, Cambridge, GB

Pecha P, Pechova E (2005) Modeling of random activity concentration fields in air …. HARMO10 Conf., Sissi (Crete),Greece, October 17–20, 2005, paper No. H11–069

Pianosi F, Beven K, Freer J, Hall JW, Rougier J (2016) Sensitivity analysis of environmental models: a systematic review with practical workflow. Environ Model Softw 79:214–232

Rakesh PT, Venkatesan R, Srinivas CV, Baskaran R, Venkatraman B (2019) Performance evaluation of modified Gaussian and Lagrangian models under low wind speed: a case study. Ann Nucl Energy 133:562–567

Razavi S, Gupta HV (2015) What do we mean by sensitivity analysis? The need for comprehensive characterization of "global" sensitivity in earth and environmental systems models. Water Resour Res 51:3070–3092

Saltelli A, Annoni P (2010) How to avoid a perfunctory sensitivity analysis. Environ Modell Softw 25(12):1508

Saltelli A, Chan K, Scott EM (2001) Sensitivity analysis. John Wiley & Sons Ltd., Hobooken

Saltelli A, Annoni P, Azzini I, Campolongo F, Ratto M, Tarantola S (2010) Variance based sensitivity analysis of model output. Design and estimator for the total sensitivity index. Comp Physics Communications 181:259–270

Saltelli A, Aleksankina K, Becker W, Fennell P, Ferretti F, Holst N, Sushan L, Wu Q (2019) Why so many published sensitivity analyses are false? A systematic review of sensitivity analysis practices. Environ Model Softw 114:29–39

Sarrazin F, Pianosi F, Wagener T (2016) Global sensitivity analysis of environmental models: convergence and validation. Environ Model Softw 79(2016):135–152

Zannetti P (1990) Air pollution modeling. theories, computational methods and available software. ISBN 1 – 85312–100–2